

Copyright © IJCESEN

International Journal of Computational and Experimental Science and ENgineering (IJCESEN)

Vol. 11-No.4 (2025) pp. 9114-9122 http://www.ijcesen.com

Research Article



ISSN: 2149-9144

Study of the Influence of Different Welding Parameters on the Mechanical behaviour of Metallic Structures

Mohamed Benziane 1*, Mokhtar Zemri², Riad Brahami³, Mohamed Bouamama⁴

¹ Mechanical Engineering Department, Laboratoire de Matériaux et Systems Réactis (LMSR), University of Sidi Bel Abbes, Sidi Bel Abbes, 22000, Algeria

* Corresponding Author Email: benzianemohamed22@yahoo.fr - ORCID: 0000-0002-5247-0050

²Mechanical Engineering Department, Laboratoire de Matériaux et Systems Réactis (LMSR), University of Sidi Bel Abbes, Sidi Bel Abbes, 22000, Algeria

Email: mokhta2r@gmail.com- ORCID: 0000-0002-5247-1440

³Center of Research in Mechanics (CRM), BP N73B, Ain El Bey, Constantine, Algeria

Email: ria2d@gmail.com- ORCID: 0000-0002-5247-1880

⁴Center of Research in Mechanics (CRM), BP N73B, Ain El Bey, Constantine, Algeria **Email:** bouamam2a@gmail.com- **ORCID:** 0000-0002-5247-1340

Article Info:

DOI: 10.22399/ijcesen.4371 **Received:** 05 September 2025 **Revised:** 10 November 2025 **Accepted:** 24 November 2025

Keywords

Welding Residual Stress Energy Release Rate Stress Intensity

Abstract:

Assessing the integrity of a structure involves demonstrating its ability to perform its mechanical functions under all normal or accidental stresses throughout its service life. In the gas safety sector, for major installations such as tanks or primary circuits, deterioration can be identified in several areas, such as cracks caused during the welding process. The aim is therefore to prove the mechanical strength of the structure in the event of this type of failure. We also aim to modify the strength of a structure when a crack is present and anomalies have been identified during an inspection. In this context, fracture mechanics theory provides the necessary tools to study cracked elements. The objective is to establish a fracture criterion that will make it possible to determine in advance the stress margins in normal or accident situations during operation. It is necessary to specifically characterise each type of fracture.

1. Introduction

Mechanical behaviour refers to all the reactions of a material or structure subjected to external stresses: tensile, compressive, bending, shear or torsional forces. For metal structures, this behaviour depends heavily on the intrinsic properties of the metal used (yield strength, tensile strength, Young's modulus, etc.), but also on the structural condition of the material after processing (welding, heat treatment, rolling, etc.).

When subjected to stress, metal structures can exhibit various phenomena such as elastic deformation, plasticity, brittle or ductile fracture, fatigue, or creep at high temperatures. These mechanical responses are influenced by multiple factors, including loading conditions, part geometry, assembly types, and heterogeneities introduced by manufacturing processes such as welding.

Welding processes cause changes in microstructure, residual stresses and distortions that play an essential role in the mechanical strength of assemblies. These stresses and deformations mainly result from temperature gradients and phase transformations that can occur during the process. The benefits of welding modelling are as follows:

- Feasibility studies of a process to identify any structural misalignment or optimise the welding sequence.
- Assessment of the mechanical strength of welded assemblies.

The feasibility of a process is assessed in terms of residual deformations. Evaluating these deformations requires simulations on the structure, including all welded assemblies.

[1] Radialisation: a numerical simulation of a welded steel joint [2] A48AP steel Experimental study [3] Study of the influence of metal structure on the machinability of steels [4] The welding process

is modelled [5] finite element method with isoparametric quadrilateral elements with eight nodes[6] main crack initiation mechanisms [7] welding processes[8], modelling mechanical behaviour and fatigue resistance [9] residual stresses calculated by the numerical method presented are consistent [10] The effects of welding parameters [11] Analysis of the welding process based on the thermoelastic-plastic equation [12] The mechanical behaviour of TIG-welded sheets is assessed on the basis of tensile tests [13]. Digital tools have initially enabled a better understanding of the physical phenomena [14] and the evolution of cracks during fatigue [15]. The mechanical model is developed in ABAQUS/ Explicit and the various opportunities[16] The evolution and strength of HLE steel pipes of grade X60M API5L and their performance after the welding process[17] Comparison between experimental and calculated values[18] Finite element modelling of distortion due to welding a T-joint [19] Calculation of residual stresses due to welding using the finite element method[20] Measurement of residual stresses due to welding and welding—this study examines the effect of hammering on these stresses. The measurement method used is the contour method, which analyses stress relaxation after EDM cutting. Laser-measured displacements are used to determine normal stresses. This method will be applied to A516 carbon steel plates, both welded and hammered. The aim of this work is to compare the mechanical behaviour of welded and unwelded metal specimens through numerical simulations reproducing tensile, bending and fatigue tests. The objective is to evaluate the impact of welding on strength, Young's modulus and crack propagation speed in order to identify critical areas and optimise process conditions to improve the reliability of industrial metal structures.

2. General Presentation of the Material

The material used is X60, the raw material is supplied by Tréfilage et de fabrication des produits de soudage 'TREFISOUD', a subsidiary of ENTPL, to SARL CITER-GAZ/Mascara.

The weld joint used in the rest of the study was electric arc welded in accordance with API1104 and a welding procedure.

A chemical analysis (Table 1) was carried out at the company's research centre. The chemical composition of the steel in question is as follows.

 Table 1. Chemical composition of X60

Table 1. Chemical composition of X00								
Materi	C	Si	Mn	S %	Cr	Cu	Ti	Fe
al	%	%	%		%	%	%	%
X60	0.08	0.236	1.243	0.007	0.136	0.019	0.016	98.15

Mechanical properties (Table 2) were tested at the company's research centre, steel.

Table 2. Mechanical properties of X60.

Yield strength (MPa)	415 – 460
Tensile strength (MPa)	520 - 760
Elongation A (%)	20 – 28
Modulus of elasticity (GPa)	200 – 210
Poisson's ratio	0.29 - 0.30
Hardness (HB)	180 – 220
Impact energy (J at 0 °C)	≥ 27
Density (kg/m³)	≈ 7850

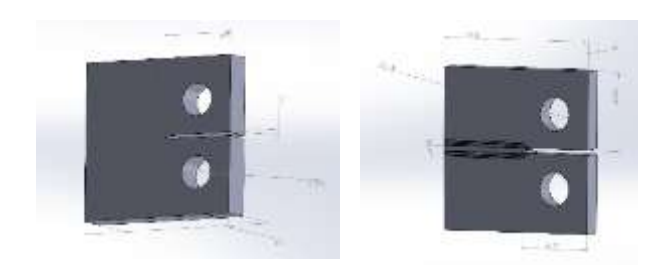
X60 steel is a low-alloy, low-carbon steel that combines good mechanical strength with excellent weldability. Its balanced composition, dominated by iron, manganese and low carbon content, gives it both strength and ductility. Its mechanical properties — yield strength of 415–460 MPa, tensile strength of 520–760 MPa and elongation of 20–28% — demonstrate that it is both strong and tough. Thanks to its good toughness (≥27 J at 0 °C) and moderate hardness, it is particularly suitable for demanding applications such as gas and oil transport pipelines.

3. Methodology of Numerical Simulation

The methodology adopted for the numerical simulation of a crack involves two types of steel test specimens:

- The first is made of homogeneous, isotropic steel material.
- The second has an area welded using filler metal.

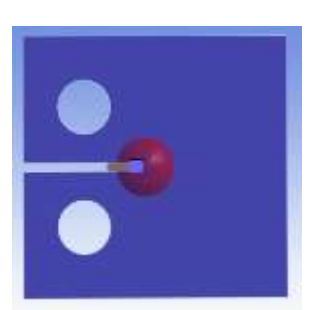
Figure 1 (a) (b) For The process begins with three-dimensional (3D) numerical modelling.

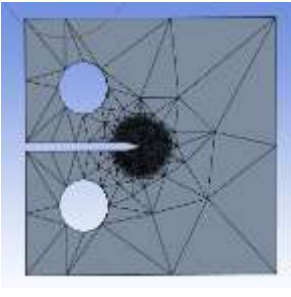


(a) unwelded (b) welded Figure 1. Fatigue test specimen (3D).

And for the welded test specimen: More X60 material with the parameters shown above the E6010

filler metal parameters. Figure 2 (a) For body size, the mesh refinement in the crack initiation zone is done with a sphere radius of 0.9 mm and an element size of 0.4 mm radius.



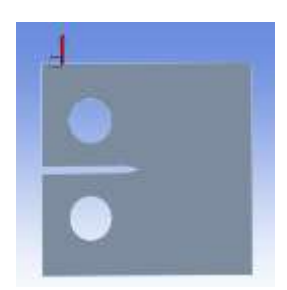


(a) crack initiation zone (b) quadratic mesh

Figure 2. Quadratic mesh type with the priming zone.

For the crack propagation parameters, we used 'Smart crack propagation' and "Fatigue" as the crack propagation option, applying the 'Paris law' and using the 'Life prediction' crack propagation method.

Figure 3 shows the boundary conditions: Application of a force of 200 N, which is effectively the maximum force, so experimentally we work with a percentage of 65 to 80% of the elastic limit. This is approximately 7 and 8 kN.



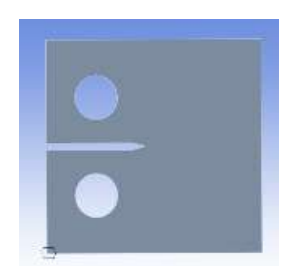


Figure 3. boundary conditions.

A numerical simulation using the finite element method was performed to study the mechanical behaviour of X60 steel in welded and unwelded states. The geometric model, based on the standard dimensions of the test piece, distinguishes the welded area from the base metal, with a refined mesh in critical areas. The mechanical properties (Young's modulus, Poisson's ratio, yield strength and plastic law) were integrated, and the boundary conditions faithfully reproduced the experimental test. The results will enable the distribution of stresses and strains to be analysed and the stress-strain curves from the simulations and acétal tests to be compared.

4. Extraction des Valeurs

This expression links material deformations to nodal displacements via the deformation matrix [B], also known as the compatibility matrix.

Stress-strain Material behaviour

$$\sigma = [D] \varepsilon = E\varepsilon \tag{1}$$

 σ : stress vector, ε : strain vector, [D]: stiffness matrix (or elasticity matrix).

Determine Young's modulus

$$\sigma = E\varepsilon = E[B]\{ue\} \tag{2}$$

E is the modulus of elasticity and [B] is the deformation matrix relating $\varepsilon = [B]\{ue\}$

Effort–strain relationship

$$\{F\} = \int_{V} [B]^{T} \{\sigma\} dV \qquad (3)$$

 $\{F\}$ is the vector of equivalent nodal forces, [B] is the deformation matrix, $\{\sigma\}$ is the stress vector, and V is the volume of the element.

Hollomon's law is:

$$\sigma = K \varepsilon n \tag{4}$$

σ: true stress (MPa), ε: true strain (unitless), K: consistency coefficient (MPa), n: work hardening exponent.

The most commonly used law for modelling fatigue resistance is Basquin's law:

$$\sigma_a = \sigma_f'(2N_f)^b \tag{5}$$

 σ_a is the stress amplitude, σ_f' is the true fatigue stress (or endurance stress), N_f s the number of cycles to failure, and b is the characteristic fatigue exponent of the material.

Or in logarithmic form (more practical for graphs):

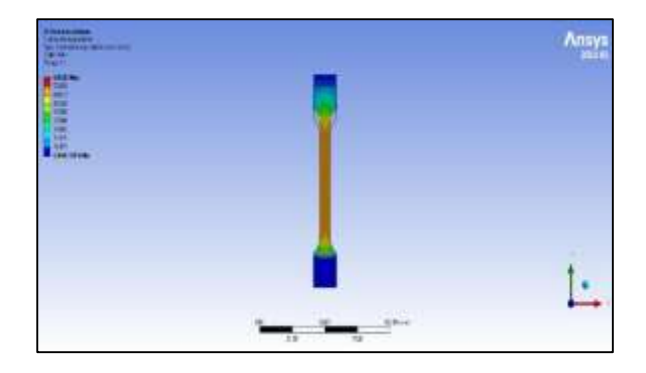
$$\log \sigma_a = \log \sigma_f' + b \log(2N_f)$$
 (6)

 σ_a : stress amplitude (value of the stress applied in fatigue), σ_f' : true fatigue stress (or endurance stress, characteristic of the material), N_f : number of cycles to failure (service life in cycles), b: fatigue exponent (describes the slope of the Wöhler/fatigue curve).

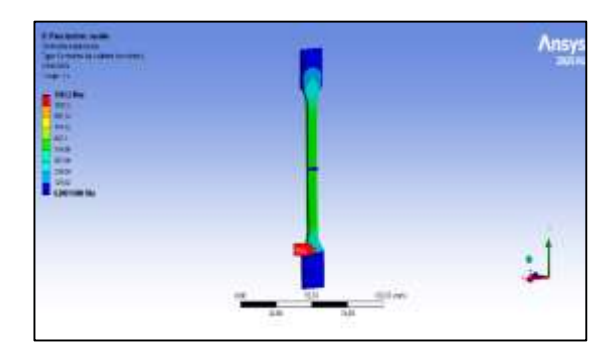
5. Results and Discussions

Numerical modelling was performed using Ansys software to examine the mechanical behaviour of welded and unweded metal specimens made of X60 steel subjected to three specific tests: tensile, bending and fatigue. A standardised three-dimensional model was designed for each test, using boundary conditions identical to those implemented experimentally. The tensile test was used to determine the elastic limit and ultimate strength of the material, while the bending test highlighted the impact of the welded area on stiffness and stress distribution. The fatigue study examined the durability of the material under cyclic loading and determined the number of cycles to failure.

Figure 4 shows the equivalent stresses in a non-welded (a) and welded (b) metal test piece made of X60 steel subjected to tensile stress.



(a) unwelded



(b) welded

Figure 4. Presentation of equivalent stresses for test specimens (a) and (b)

Figure 5 illustrates a comparison of the tensile curves (stress-strain) obtained during tensile testing for unwelded and welded X60 steel test specimens. If you need subsection you should do it using this format.

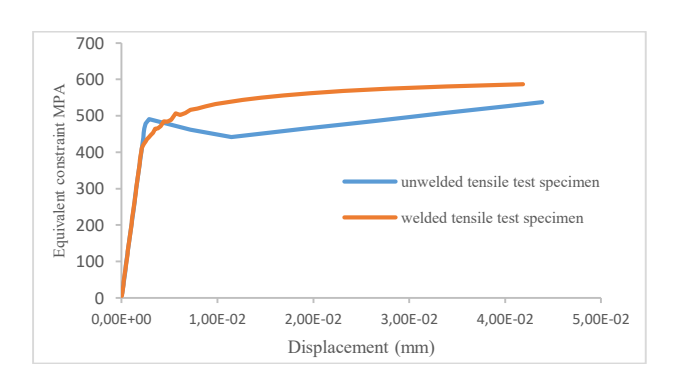


Figure 5. presentation of the tensile curves of a test piece.

Table 3. Mechanical properties of X60 numerical calculation.

-	Test tube	Poisson's ratio	Hardness (HB)	Impact energy (J at 0 °C)	Density (kg/m³)
	unwelded	0,30.	198	45	7850
	welded	0,30.	207	24	7850

Analysis of the stress-strain curves obtained for the unwelded and welded test pieces reveals marked differences in the mechanical behaviour of X60 steel. In the elastic stage, the initial decline in the

modulus curves indicates Young's approximately 195,145 MPa and 195,157 MPa, a characteristic value for steel used in construction. The welded test piece has a higher elastic limit and maximum strength than the unwelded test piece, reaching approximately 411 MPa and 427 MPa respectively. The elongation of the unwelded test piece is 30% and 20% for the welded test piece. This increase in strength is attributed to the metallurgical modification of the molten metal and the hardening effect induced by the welding thermal cycle. On the other hand, the plastic zone of the curve shows a reduction in the ductility of the welded test piece, reflecting a lower capacity for deformation before fracture. These results confirm that welding significantly influences the mechanical properties of X60 steel, increasing its strength while reducing the flexibility of the material. Figure 6 shows the total displacements of an unwelded and welded metal test piece made of X60 steel subjected to three-point bending.

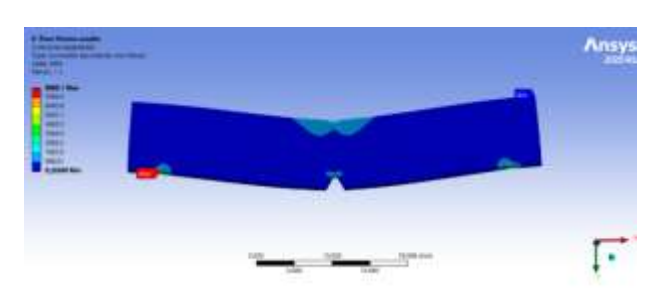


Figure 6. Presentation of 3-point bending test (equivalent stresses).

Figure 7 illustrates the comparison of the elastic stress–strain curves obtained during bending tests for unwelded and welded X60 steel specimens.

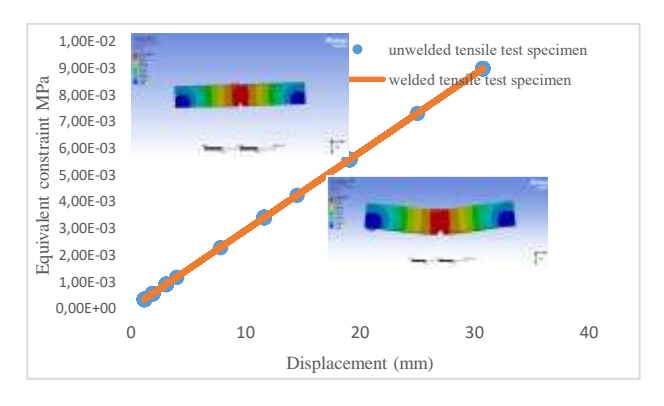


Figure 7. Presentation of three-point bending curves with displacement of an unwelded and welded test piece.

Figure 7 shows a linear relationship between equivalent stress and displacement for both test pieces, indicating that the material behaviour remains elastic within the range studied. The study focused mainly on the initial part of the elastic behaviour, as this illustrates the most important

phase for determining the stiffness and modulus of elasticity of the material. This zone allows the linear reaction of the metal to be defined before any plastic deformation occurs. The data indicate that the mechanical strength remains virtually the same for both welded and unwelded types throughout the elastic phase. The curves show a parallel development, indicating a notable similarity in elastic behaviour and confirming that the presence of the weld does not have a significant impact on the initial stiffness of the material. Figure 8 shows the equivalent stresses in a non-welded and welded metal test piece made of X60 steel subjected to fatigue.

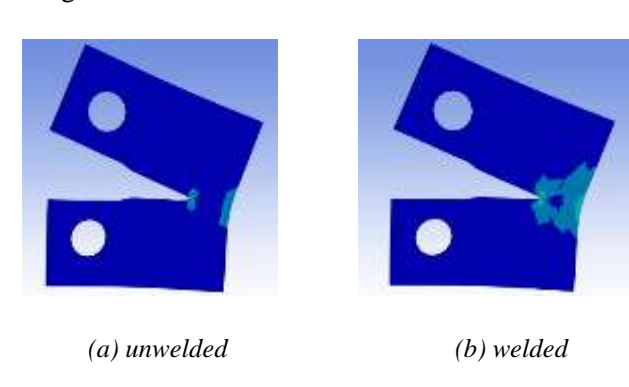


Figure 8. Fatigue test presentation (a) and (b) equivalent stresses of a test piece.

Figure 9 illustrates the comparison of crack propagation behaviour between types of test pieces obtained during fatigue tests for non-welded and welded X60 steel test pieces.

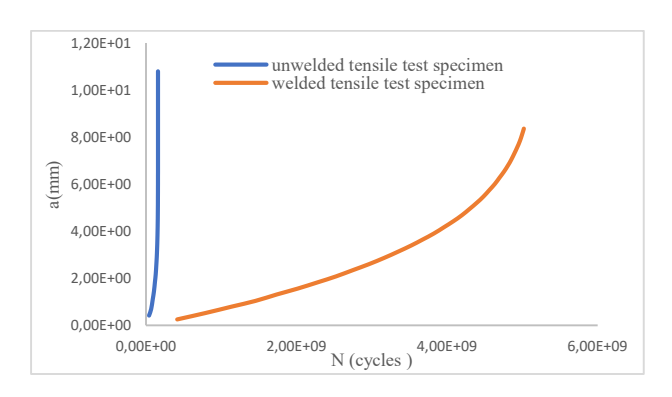


Figure 9. Presentation of crack propagation behaviour curves for a non-welded and welded test piece.

Figure 9 shows the evolution of crack length a (mm) as a function of the number of cycles N for welded and non-welded test pieces subjected to fatigue testing. It can be seen that the crack propagates much more rapidly in the unwelded test piece, whose curve shows a sudden increase over a very small number of cycles, indicating an almost instantaneous fracture. Conversely, the welded test

piece shows slower and more gradual crack propagation, extending over a large number of cycles, which reflects better fatigue resistance or a longer life before fracture. Thus, welding appears to give the material an increased ability to delay crack growth under cyclic loading. Figure 10 illustrates the comparison of crack propagation between types of specimens obtained during fatigue testing for unwelded and welded X60 steel specimens.

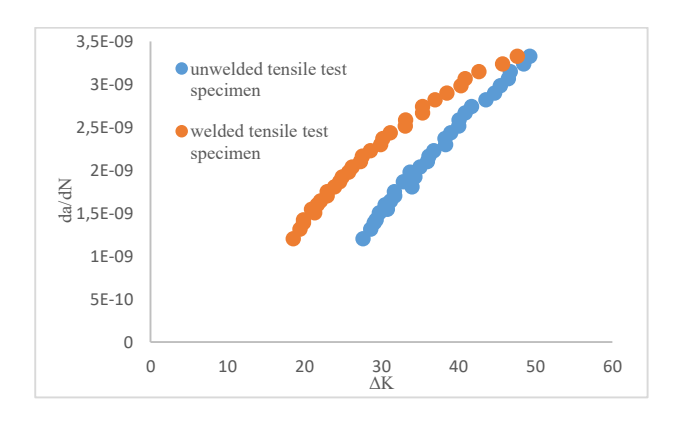


Figure 10. Presentation of crack propagation curves (Paris law)

Figure 10 illustrates the fatigue crack propagation rate (da/dN) as a function of the stress intensity factor amplitude (ΔK) for welded and non-welded test pieces. It can be seen that, for the same value of ΔK , the crack growth rate is higher in the welded test piece than in the unwelded test piece. This indicates that welding makes the material more susceptible to crack propagation under cyclic loading, probably due to the presence of residual stresses, microstructural defects or heterogeneities in the heat-affected zone. In contrast, the unwelded test piece présente une propagation plus lente, traduisant une meilleure résistance à la fatigue. Globalement, cette figure montre que, Although welded material may have a high overall service life, its crack propagation rate at a given stress is faster than that of unwelded material.

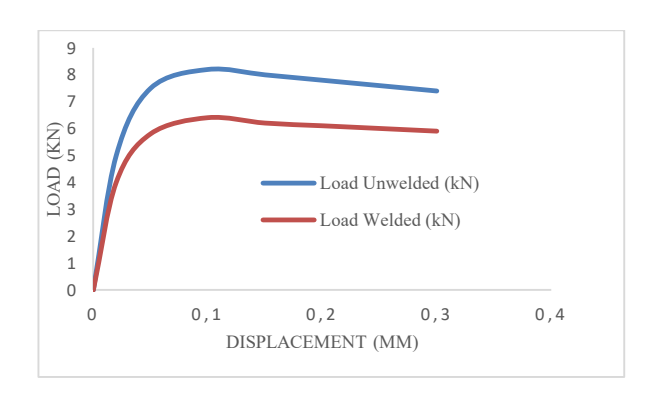


Figure 11. Presentation of load and displacement curves.

Figure 11 illustrates the load curve as a function of displacement for two test specimens, one welded and one unwelded. It can be seen that the curve for the unwelded test piece has a steeper initial slope and reaches a maximum load of approximately 8.3 kN. This shows that its strength and stiffness are better. However, the welded test piece has a maximum load that is approximately 6.0 kN lower, suggesting a reduction in mechanical strength due to the presence of the weld. Once the maximum load is reached, the unwelded curve shows a slight decrease in load, indicating increased ductility. In contrast, the welded curve stabilises quickly, suggesting reduced ductility. In conclusion, welding degrades the mechanical properties of the material, reducing both its strength and its plastic deformation capacity.

6. Evaluation of Results

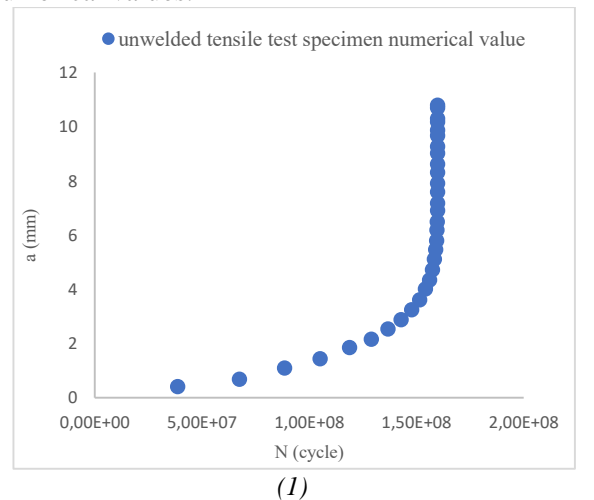
Table 04 shows the mechanical properties of X60 steel for an unwelded test piece, comparing experimental and numerical values.

Table 4. Mechanical properties of X60 steel tensile test.

Results	Young's modulus E (MPa)	Yield strength Re (MPa)	Ultimate strength Rm(Mpa	A %	n	K
Experiment al (unsoldered test piece)	200000	414.00	525.0	25	0.05	57 8
Unsoldered test piece (Numerical)	19514 5	427.6	491.0 7	30	0.04 9	65 0

The results presented show a good correlation between the experimental and numerical values for the unwelded test piece, confirming the reliability of the results. The Young's modulus, calculated numerically (195,145 MPa), is very close to the experimental value (200,000 MPa). This shows that the stiffness of the material is well reproduced by the model. The simulated yield strength (427.62 MPa) is slightly higher than the measured value (414 MPa), which reflects a slight overestimation of the strength at the onset of plasticity. However, the ultimate strength is slightly underestimated (491.07 MPa versus 525 MPa), which can be attributed to simplifications in the modelling of plastic behaviour. The elongation at break is higher in the simulation (30% versus 25%), suggesting slightly higher ductility. Finally, the work hardening coefficients n and K are close, confirming the consistency of the modelled plastic behaviour. These results indicate that the numerical simulation accurately reproduces the overall mechanical behaviour of the unwelded test piece, with small and acceptable deviations.

Figure 12 shows the evolution of crack length (a) as a function of the number of cycles (N) for an unwelded test piece, comparing experimental and numerical values.



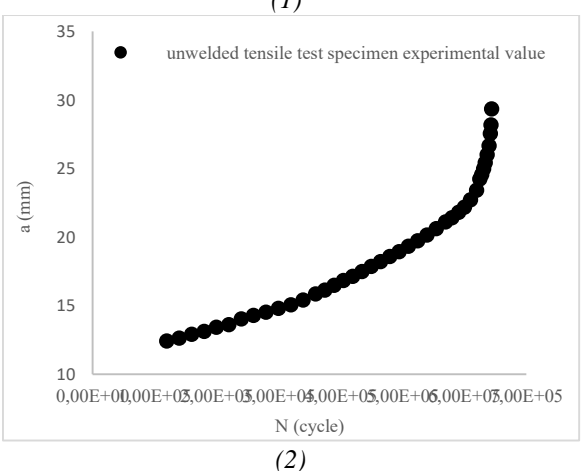
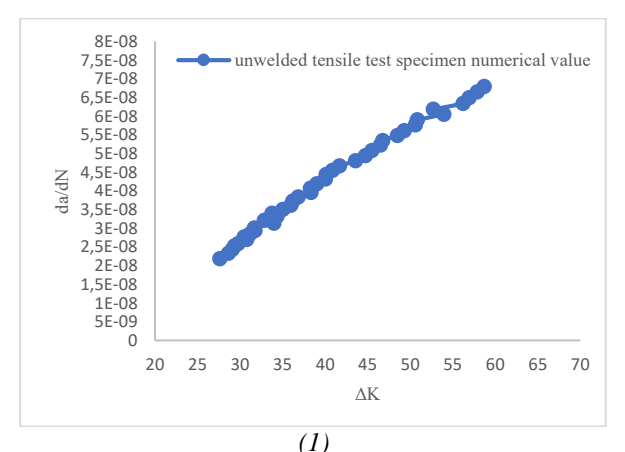


Figure 12. Presentation of load and displacement curves.

It can be observed that, in both cases, the crack remains stable for most of the number of cycles, then grows rapidly at the end of the material's life. The experimental curve shows slightly faster crack propagation and a greater final length than in the numerical simulation. This indicates that the numerical model slightly underestimates the crack propagation speed, probably due approximation of the growth law used or a difference in the loading conditions applied. Overall, the general trend is well reproduced: the crack evolves slowly during the initiation phase, then accelerates sharply before fracture. This consistency between the two curves shows that the simulation correctly describes the fatigue behaviour with good accuracy, despite a slight underestimation of the actual propagation. Figure 13 shows the evolution of the propagation rate da/dN as a function of the stress intensity factor ΔK on a log-log scale for an unwelded test piece, comparing experimental and numerical



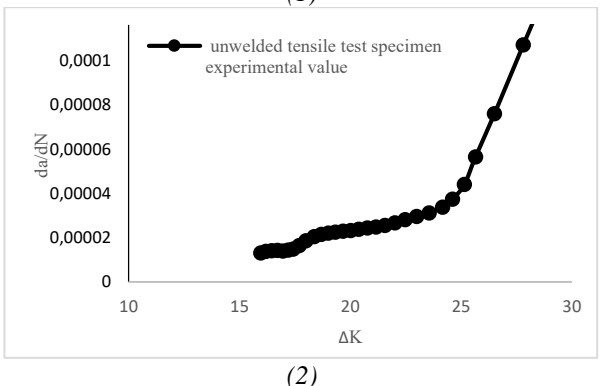


Figure 13. Presentation of crack propagation curves (Paris law).

In the numerical simulation, the curve shows a steady and gradual evolution of da/dN. The increase in ΔK reflects a more regular and predictable behaviour of the model. Furthermore, the experimental results indicate a more abrupt increase in crack propagation speed above a certain ΔK threshold, suggesting a transition to unstable crack propagation. A comparison of the two trends reveals good qualitative consistency, but the experimental values show behaviour that is more sensitive to local variations and actual material imperfections than the numerical model results. Figure 14 presents a comparison between the two numerical and experimental values for the fatigue behaviour of the unwelded test piece.

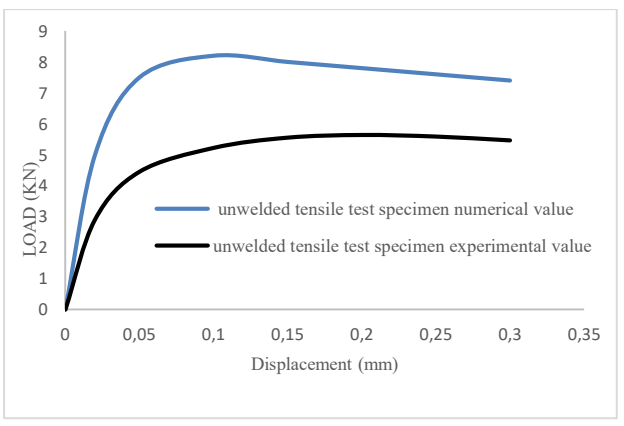


Figure 14. Presentation of load and displacement curves

During a fatigue test, the experimental and numerical results for the unwelded test piece were compared. This showed that Hollomon's law accurately predicts the overall behaviour. Initially, the load increases rapidly, then stabilises, which corresponds to a work hardening phase of the material. The two curves follow the same trend. However, the numerical curve reaches higher maximum loads, reflecting an overestimation of the material's strength by the Hollomon model. This difference can be attributed to model parameters (the strength coefficient K and the work hardening exponent n) that are slightly higher than those observed under actual fatigue conditions. On the other hand, the general trend is well reproduced, particularly in the initial elastic phase, where the slopes are comparable, indicating a consistent Young's modulus. Hollomon's law therefore adequately describes the cyclic behaviour of unwelded material under fatigue, while requiring fine adjustment of the parameters to accurately reflect the experimental response.

7. Conclusions

The main objective of the in-depth study conducted on X60 steel was to assess the influence of welding on mechanical behaviour, crack propagation and fatigue resistance, in order to validate our model of unwelded test pieces by comparing numerical values with experimental ones. The unwelded test piece and the experimental test piece demonstrated more consistent behaviour, reflecting better mechanical stability. The results from the numerical simulation of the tensile, bending and fatigue tests for both welded and unwelded test pieces (base metal) identified several notable differences between these configurations. Firstly, the modulus of elasticity (E) remains virtually unchanged for both specimens, indicating that the overall stiffness of the material is not significantly affected by the welding process. However, the values for the yield strength (Re) and ultimate strength (Rm) vary significantly: the welded test piece shows a slightly higher ultimate strength, but this comes at the expense of its ductility, which decreases to 20% elongation, while the unwelded test piece shows 30%. This loss of ductility is due to the presence of residual stresses, metallurgical transformations in the heat-affected zone, and a more brittle microstructure around the weld joint. Load-displacement curves confirmed this trend by showing a reduction in the maximum load supported by the welded material, reflecting a decrease in toughness and earlier fracture. The unwelded and welded test pieces demonstrated more consistent behaviour, reflecting better mechanical stability. Furthermore, the study

propagation, according to Paris's law, revealed a higher propagation speed for the welded test piece, illustrating its lower fatigue resistance. These differences can be explained by the heterogeneous structure created during welding, significant thermal gradients and the non-uniform distribution of internal stresses, which cause local alteration of the mechanical properties, affecting the durability and crack resistance of X60 steel. Welding reduces the mechanical strength and fatigue resistance of the material. In conclusion, this study clearly shows that welding the test piece results in faster crack propagation, lower maximum load and reduced ductility. These consequences are due to residual stresses and welding-related defects. The overall performance of the unwelded material is therefore better, both in terms of strength and durability.

Author Statements:

- Ethical approval: The conducted research is not related to either human or animal use.
- Conflict of interest: The authors declare that they have no known competing financial interests or personal relationships that could have appeared to influence the work reported in this paper
- Acknowledgement: The authors declare that they have nobody or no-company to acknowledge.
- **Author contributions:** The authors declare that they have equal right on this paper.
- **Funding information:** The authors declare that there is no funding to be acknowledged.
- Data availability statement: The data that support the findings of this study are available on request from the corresponding author. The data are not publicly available due to privacy or ethical restrictions.

References

- [1] AHMED, B., El Bahri, O. C., Benattou, B., & Malika, T. (2018). Numerical Simulation of a Steel Weld Joint and Fracture Mechanics Study of a Compact Tension Specimen for Zones of Weld Joint. Fracture and Structural Integrity, 13(47), 17–29. https://doi.org/10.3221/IGF-ESIS.47.02
- [2] Alioua, A., Bouchouicha, B., & Zemri, M. (2012). Experimental study of A48AP steel [Research thesis]. Djillali Liabès University, Sidi Bel Abbès, Algeria.
- [3] Haddad, F. (2020). Study of the influence of metallurgical structure on the machinability of high mechanical strength steels [Doctoral thesis, HESAM University].
- [4] Kouider, N., et al. (2019). Modeling of the welding process. Revue des Sciences et Technologies Synthèse, 25(2), 116–128. https://biblio.univ-

- annaba.dz/wp-content/uploads/2022/12/These-Kouider-Nadia.pdf.
- [5] Oubraham, C., Benyounes, K., Sahoui, H., & Benmounah, A. (2014). Modeling and simulation of the response of elements in metallic structures influenced by shear parameters. In Proceedings of the 4th International Conference on Welding, No-Destructive Testing and Materials and Alloys Industry (IC-WNDT-MI'14).
- [6] Demmouche, Y. (2012). Study of the fatigue behavior of FSW welded assemblies for aeronautical applications (Doctoral dissertation, Ecole nationale supérieure d'arts et métiers-ENSAM).
- [7] Mezrag, B. (2015). Study of the influence of welding parameters on the microstructure and mechanical behavior of steel-aluminum assemblies obtained by MIG-CMT arc welding (Doctoral dissertation, University of Montpellier; Aboubekr Belkaid University of Tlemcen (Tlemcen, Algeria).
- [8] Truant, X. (2018). Study and modeling of the mechanical behavior of friction-stir welded (FSW) structural panels (Doctoral dissertation, Université Paris sciences et lettres).
- [9] Shoheib, M. M., Shahrooi, S., Shishehsaz, M., & Hamzehei, M. (2022). Fatigue crack propagation of welded steel pipeline under cyclic internal pressure by Bézier extraction based XIGA. *Journal of Pipeline Systems Engineering and Practice*, 13(2), 04022001.
- [10] Taibi, A. (1993). Study of the influence of continuous CO2 laser welding parameters on the spectral and temporal emission of the welding plasma: Application to 304L stainless steel, Ti40 titanium and aluminum (Doctoral dissertation, Lyon, INSA).
- [11] Shoheib, M. M., Shahrooi, S., Shishehsaz, M., & Hamzehei, M. (2023). The application of the isogeometric method based on bézier extraction for the thermo-plastic analysis of welded steel plate. *Mechanics of Solids*, 58(1), 245-265.
- [12] AISSANI, M. (2013). Study of the thermal and mechanical behavior of aeronautical materials by numerical methods: application to the welding of metallic structures (Doctoral dissertation, Saad Dahlab University-Blida 1).
- [13] Saadlaoui, Y., Sijobert, J., Doubenskaia, M., Bertrand, P., Feulvarch, E., & Bergheau, J. M. (2020). Experimental study of thermomechanical processes: Laser welding and melting of a powder bed. *Crystals*, 10(4), 246.
- [14] Athanassiadis, A., Boissenot, JM, Brevet, P., Francois, D., & Raharinaivo, A. (1981). Calculs de mécanique de la rupture élastique linéaire de corps cylindriques fissurés soumis à une tension. *International Journal of Fracture*, 17 (6), 553-566.
- [15] Guglielmetti, A. (2012). Numerical study of magnetic pulse welding. University of Quebec at Chicoutimi.
- [16] MERZOUG, M., & MAZARI, M. (2015). Parametric study of friction stir welding (Doctoral dissertation).

- [17] Nyankam, T. C. T. (2016). Multi-physics modeling of the welding arc and weld bead deposition during a welding operation: prediction of distortions and residual stresses (Doctoral dissertation, University of Technology of Belfort-Montbeliard).
- [18] Kassab, R. K. (2007). Finite element method modeling of distortions due to welding of a T-joint (Doctoral dissertation, École de technologie supérieure).
- [19] Morin, O. (2006). Calculation of residual stresses due to welding by the finite element method (Doctoral dissertation, École de technologie supérieure).
- [20] Nasri, H. (2007). Measurement of residual stresses due to welding and hammer-welding by surface micro-profile (Doctoral dissertation, École de technologie supérieure).